Accepted Manuscript

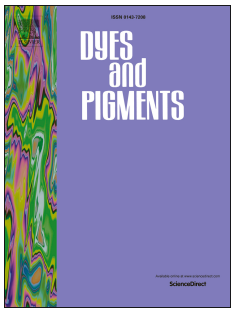

Synthesis and biological imaging of fluorescent polymeric nanoparticles with AIE feature via the combination of RAFT polymerization and post-polymerization modification

Yanzhu Liu, Liucheng Mao, Saijiao Yang, Meiying Liu, Hongye Huang, Yuanqing Wen, Fengjie Deng, Yongxiu Li, Xiaoyong Zhang, Yen Wei

PII: S0143-7208(17)32404-X

DOI: 10.1016/j.dyepig.2018.05.032

Reference: DYPI 6761

To appear in: *Dyes and Pigments*

Received Date: 21 November 2017

Revised Date: 15 May 2018

Accepted Date: 15 May 2018

Please cite this article as: Liu Y, Mao L, Yang S, Liu M, Huang H, Wen Y, Deng F, Li Y, Zhang X, Wei Y, Synthesis and biological imaging of fluorescent polymeric nanoparticles with AIE feature via the combination of RAFT polymerization and post-polymerization modification, *Dyes and Pigments* (2018), doi: 10.1016/j.dyepig.2018.05.032.

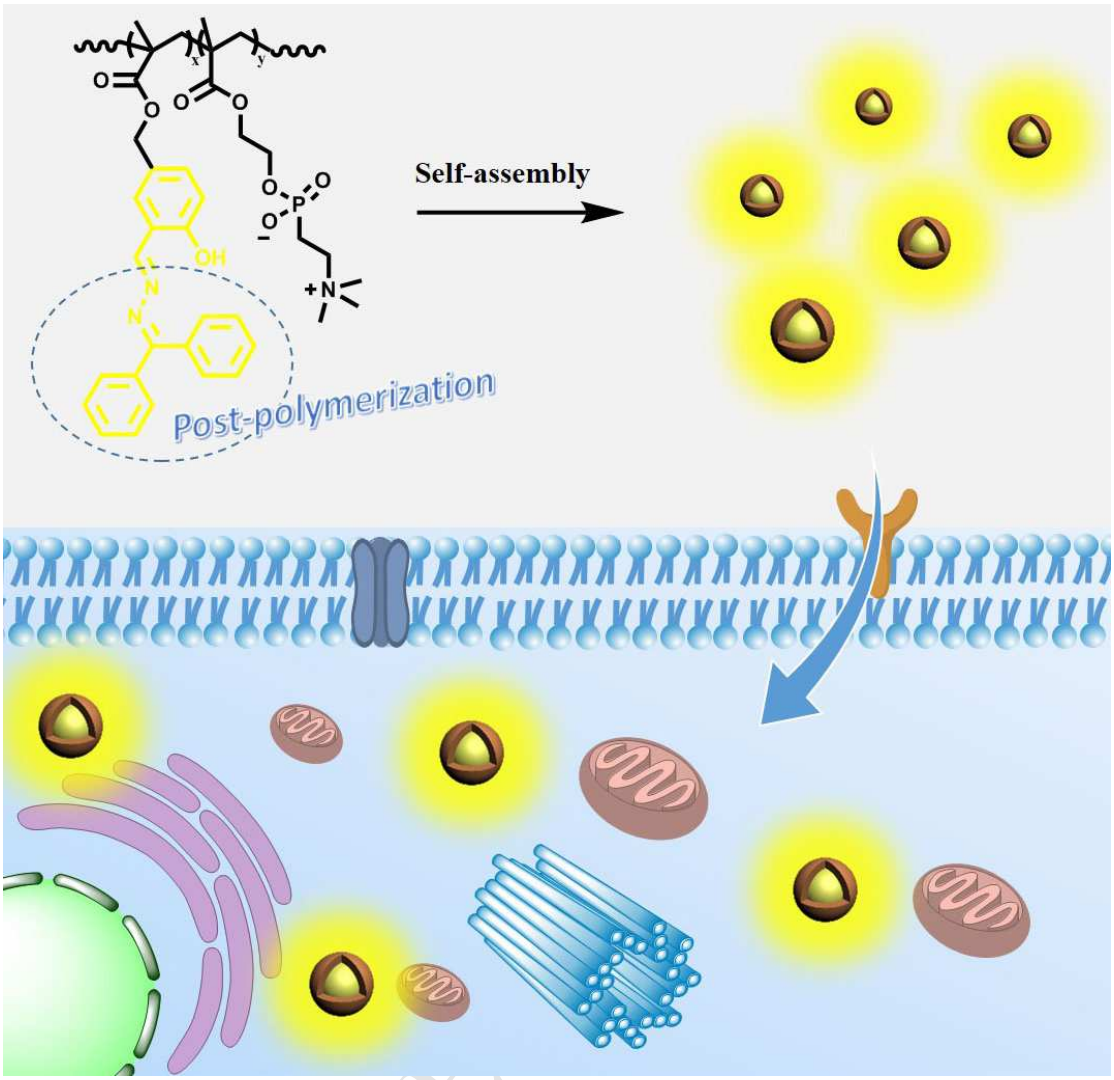

A novel strategy based on the combination of RAFT polymerization and post-polymerization has been developed for the synthesis of fluorescent polymeric nanoparticles with ESIPT feature

Synthesis and biological imaging of fluorescent polymeric nanoparticles with AIE feature via the combination of RAFT polymerization and post-polymerization modification

Yanzhu Liu[a,#], Liucheng Mao[a,#], Saijiao Yang[a], Meiying Liu[a], Hongye Huang[a], Yuanqing Wen[a], Fengjie Deng[a], Yongxiu Li[a,*], Xiaoyong Zhang[a,*], Yen Wei[b,c,*]

[a] Department of Chemistry, Nanchang University, 999 Xuefu Avenue, Nanchang 330031, China.

[b] Department of Chemistry and the Tsinghua Center for Frontier Polymer Research, Tsinghua University, Beijing, 100084, P. R. China.

c Department of Chemistry and Center for Nanotechnology and Institute of Biomedical Technology, Chung-Yuan Christian University, Chung-Li 32023, Taiwan

# These authors contributed equally to this work

Abstract

In recent years, florescent polymeric nanoparticles (FPNs) containing aggregation-induced emission (AIE) fluorogens have received great intention for their potential applications in biological imaging and theranostic nanomedicine. Herein, we have developed AIE-active FPNs through a combination of reversible addition-fragmentation chain transfer (RAFT) polymerization and post-polymerization modification strategies. The salicylaldehyde (SA) containing zwitterionic copolymers are fabricated via RAFT polymerization and further modified by benzophenone hydrazone (BPH) via Schiff base reaction. The obtained AIE-active amphiphilic copolymers BPH-poly(FHMA-*co*-MPC) can self-assemble in aqueous solution with the hydrophobic fluorogens aggregating together to form the core and the hydrophilic chains to form the protective shell. BPH-poly(FHMA-*co*-MPC) and the resulting FPNs are characterized by ^{1}H nuclear magnetic resonance spectroscopy, Fourier transform infrared spectroscopy, transmission electron microscopy and fluorescence spectroscopy. Results demonstrate that BPH-poly(FHMA-*co*-MPC) are successfully synthesized and as-prepared BPH-poly(FHMA-*co*-MPC) FPNs exhibit desirable morphology and size, good dispersibility, high brightness, remarkable photostability and large Stokes shifts. More importantly, through cytotoxicity test and cell uptake behavior, these BPH-poly(FHMA-*co*-MPC) FPNs show low toxicity and excellent cell dyeing behavior. Taken together, we have developed a facile and effective method for the fabrication of AIE-active FPNs, which display great potential for biomedical applications.

Key words: Aggregation-induced emission, post-polymerization, fluorescent polymeric nanoparticles, biological imaging

1 Introduction

Luminescent nanomaterials have attracted great attention of scientific community because of their widespread applications in optics, electronics, memory systems, biotechnology, etc.[1, 2] Among them, the development of fluorescent polymeric nanoparticles (FPNs) has aroused tremendous scientific interests because fluorescence techniques are highly sensitive and easy to operate.[3, 4] Unfortunately, most of the traditional organic molecules possess strong emission in their solution state but very weak even non emission at high concentrations or in the aggregated states. Such quenching of emission intensity could be attributed to notorious aggregation-caused quenching (ACQ) effect, which is an intractable problem for lots of practical applications such as optoelectronic devices and biomedical research.[5] Therefore, The ACQ effect has become a huge obstacle, which impels researchers to seek anti-ACQ materials with higher luminescence efficiency in the aggregated state than in the dissolved state. In 2001, Tang and co-workers discovered an unusual anti-ACQ photophysical phenomenon which is known as aggregation-induced emission (AIE).[6] Subsequently, AIE-active materials stimulate intense research interest owing to the fundamental importance and promising practical applications, and the mechanisms and technological applications of AIE materials are unceasingly developed and perfected.[1, 7, 8] For instance, restriction of intramolecular motions (RIM) as the mechanism behind AIE has been generally accepted, and various practical applications of AIE materials including optoelectronic devices, biological/chemical sensors, biological imaging and theranostics have been exploited.[9-16]

In particular, the construction of FPNs based on AIE-active dyes through both physical and chemical methods has made remarkable achievements.[17-20] At first, a class of biocompatible amphiphilic commercialized or synthesized block copolymers were utilized to construct AIE-active FPNs with good water dispersibility for various biomedical applications through a physical encapsulation strategy.[21, 22] On the other hand, a series of more robust and versatile chemical processes were employed for fabrication of AIE-active FPNs. These fall into two categories: (1) Polymerizable AIE-active dyes directly incorporate into polymers for fabrication of FNPs via different polymerization methods such as emulsion polymerization, reversible addition fragmentation chain transfer (RAFT) polymerization, and ring-opening polymerization;[23-26] (2) Functionalized AIE molecules conjugated with biocompatible macromolecules (natural carbohydrate polymers and synthetic polymers) for construction of FPNs via multifarious chemical reactions such as Schiff base condensation and multicomponent reaction.[13, 27-30] Despite many impressive advances in construction methodologies for the fabrication of AIE-active FNPs, more facile preparation strategies are still highly desirable.

Post-polymerization means is a useful methodology for the functionalization of polymers and

endowing their new properties for wide ranging applications.[31-34] The backbone of copolymers contains a moiety with latent reactivity, which can be functionalized directly by the functional group precursor.[35] In addition, Schiff base compounds have drawn extensive research attention and have been widely put into use in the fields of medicine, catalysis, analytical chemistry, etc.[36, 37] Due to enjoying the advantages of mild reaction conditions and high reaction rates, the Schiff base reaction is used for protecting various functional groups and synthesizing a series of organic ligands.[38] Moreover, the Schiff base ligands are derived by the condensation of aldehyde/ketone with a primary amine, which plays a vital role in human welfare, modern coordination and medicinal chemistry.[39] More importantly, integration of post-polymerization methods and Schiff base reaction, which can offer a rather straightforward synthesis method and readily-modified structures to fabricate some functional polymers.

In this contribution, the existing strategy for fabrication of AIE-active FPNs based on RAFT polymerization and post-polymerization modification was used to prepare salicylaldehyde (SA) containing zwitterionic copolymers were synthesized via RAFT polymerization followed by reaction with benzophenone hydrazone (BPH) by a Schiff base reaction (**Scheme 1**). Thus obtained BPH-poly(FHMA-*co*-MPC) copolymers tend to form nanoparticles in aqueous solution as a result of their amphiphilic structure. Furthermore, the structure features, photophysics properties and microscopic morphological characteristics of BPH-poly(FHMA-*co*-MPC) FPNs were determined by a variety of characterization means. The cell cytotoxicity and cell uptake behavior of thus obtained BPH-poly(FHMA-*co*-MPC) FPNs were further determined to evaluate their potential for cell imaging applications.

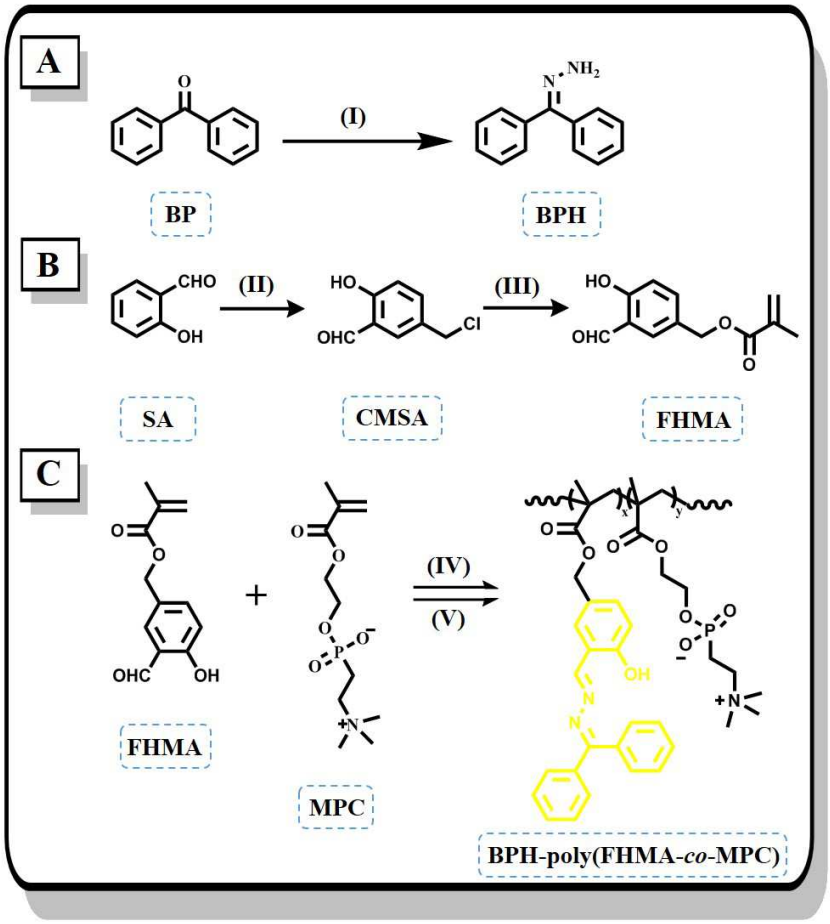

Scheme 1 Schematic illustration of the preparation procedure of BPH-poly(FHMA-*co*-MPC). (A) Synthetic route to BPH, (I) hydrazine monohydrate, 40 ºC, 24 h; (B) Synthetic route to FHMA, (II) $(CHO)_n$, rt, 24 h, (III) methacrylic acid, 50 ºC, 24 h; (C) Synthetic route to BPH-poly(FHMA-*co*-MPC), (IV) CTA, 70 ºC, 12 h, (V) BPH, 70 ºC, 4 h.

2 Experimental sections

2.1 Materials and instruments

Benzophenone (BP, *M*w: 182.22 Da, 99%), salicylaldehyde (SA, *M*w: 122.12 Da, 99%), methacrylic acid (*M*w: 86.09 Da, 99%) and absolute N,N-dimethylformamide (DMF) were purchased from Heowns Biochemical Technology Co., Ltd. (Tianjin, China). Paraformaldehyde (*M*w: 30.03, AR) and 2,2'-azobis(2-methylpropionitrile) (AIBN, *M*w: 164.21 Da, 98%) were supplied by Aladdin Reagent Co., Ltd. (Shanghai, China). 2-Methacryloyloxyethyl phosphorylcholine (MPC, *M*w: 295.27 Da, 96%) was purchased from Joy-Nature Science and Technology Development Institute. (Nanjing, China). Hydrazine monohydrate (*M*w: 32.05 Da, 99%) was supplied by TCI (Shanghai) Development Co., Ltd. Other chemicals not mentioned here were of analytical grade, and were used as received. Deionized water was used in throughout the experiments. The chain transfer agent (CTA) of

4-cyano-4-(ethylthiocarbonothioylthio) pentanoic acid was synthesized by the literature methods.[40]

^{1}H nuclear magnetic resonance (NMR) spectra were recorded on a Bruker Avance-400 spectrometer with tetramethylsilane (TMS) as the internal standard and $CDCl_3$ or d_6-DMSO as solvents. The Fourier transform infrared (FT-IR) spectra were obtained in a transmission mode on a Nicolet 5700 spectrometer (Thermo Nicolet Corporation), using powdered samples diluted in KBr pellets. The micromorphology of poly(FHMA-*co*-MPC) FPNs was investigated using a Hitachi 7650B transmission electron microscopy (TEM) operating at 80 kV. The sample for TEM measurements was prepared by dropping the solution onto a carbon-coated copper grid. The particle size of poly(FHMA-*co*-MPC) FPNs was taken on a Zeta potential analyzer (Malvern, Zetasizer nano zs90). UV−visible absorption spectra were recorded on the UV spectrometer (TU-1810, Persee) using quartz cuvettes of 1 cm path length. Fluorescence spectra were tested by a Hitachi F-4500 spectrophotometer with a slit width of 10 nm for both excitation and emission. The critical micelle concentration (CMC) was determined by the tangent method, in which ten different concentrations BPH-poly(FHMA-*co*-MPC) FPNs (0.5, 0.4, 0.3, 0.25, 0.15, 0.1, 0.05, 0.01, 0.001, 0.0001 mg mL^{-1}) were prepared for scanning fluorescent spectra (the fluorescent excitation wavelength and emission wavelength were set as 405 nm and 546 nm, respectively.).

2.2 Synthesis of benzophenone hydrazone (BPH)

BPH was synthesized via Schiff base reaction. BP (2.0 g, 11.1 mmol) was dissolved in ethanol (80 mL) at 40 ºC, followed by addition of excess hydrazine monohydrate (3.6 mL). Adding one drop of aceticacid as a catalyst before the mixture was stirred and refluxed for 24 h. After cooling to room temperature, the crude product was concentrated and then dissolved in ethyl acetate. The product was purified by washing the solution with deionized water thrice. After the organic solvent was evaporated under reduced pressure, white power of BPH was obtained in 91% yield. ^{1}H NMR (400 MHz, $CDCl_3$) δ (ppm): δ7.53-7.24 (10H, aromatic ring), 5.41 (s, 2H, -NH_2). HR-MS (ESI) calculated for $C_{13}H_{13}N_2^+$ $(M+H)^+$ 197.1073, found 197.1079. Elemental analysis calculated (%) for $C_{13}H_{12}N_2$: C 79.56, H 6.16, N 14.27, found C 78.52, H 6.40, N 14.12.

2.3 Synthesis of 3-formyl-4-hydroxybenzyl methacrylate (FHMA)

CMSA as intermediate product was prepared according to previous literature.[41] In addition, the typical experimental process for the synthesis of FHMA as following: mixture of methacrylic acid (1.72 g, 0.02 mol), NaOH (0.8 g, 0.02 mol) and deionized water (30 mL) in a 100 mL reaction bottle and the mixture were stirred at room temperature for 30 min. Subsequently, CMSA (3.41 g, 0.02 mol), KI (1.0 g, 0.002 mol) and toluene (5 mL) were added, and the solution stirred at 50 ºC for 24 h. After cooling to room temperature, the mixture was extracted with ethyl acetate (20 mL × 3), and the organic

extract was dried over anhydrous Na_2SO_4. After filtration, the solvent was removed by using a rotary evaporator. The product was purified by silica gel column chromatography with ethyl acetate: petroleum ether (v: v, 1 : 10) to give FHMA as a white crystal. Yield: 68%. ^{1}H NMR (400 MHz, $CDCl_3$) δ (ppm): δ 11.05 (s, 1H, OH), 9.91 (s, 1H, CHO), 7.61-7.55 (2H, aromatic ring), 7.00 (1H, aromatic ring), 6.14 (s, 1H, trans-CH_2), 5.60 (s, 1H, cis-CH_2), 5.16 (s, 2H, $COOCH_2$), 1.96 (s, 3H, $CH_3C=CH_2$). HR-MS (ESI) calculated for $C_{12}H_{11}O_4^-$ $(M-H)^-$ 219.0663, found 219.0660. Elemental analysis calculated (%) for $C_{12}H_{12}O_4$: C 65.45, H 5.49, O 29.06, found C 62.57, H 5.89, O 30.90.

2.4 Synthesis of BPH-poly(FHMA-*co*-MPC)

The BPH-poly(FHMA-*co*-MPC) was prepared by combining RAFT polymerization and post-polymerization method. Specifically, FHMA (110 mg, 0.5 mmol), MPC (295 mg, 1.0 mmol), CTA (28.9 mg, 0.2 mmol), AIBN (5 mg, 0.03 mmol) and absolute DMF (10 mL) were introduced into a Schlenk tube and bubbled by nitrogen flow for 30 min. The reaction mixture was stirred at 70 ºC for 12 h. After the polymerization was completed, BPH (98 mg, 0.5 mmol) was added to the reaction system. The new reaction mixture was further stirred at 70 ºC for 4 h. After cooling to room temperature, the mixture was dialyzed against water for 24 h then ethanol for 24 h using 3500 Da *M*w cutoff dialysis membranes. Finally, the resulting product was carried out by freeze-drying.

2.5 Cytotoxicity of BPH-poly(FHMA-*co*-MPC) FPNs

The cytotoxicity of as-prepared BPH-poly(FHMA-*co*-MPC) FPNs was evaluated by cell counting kit-8 (CCK-8) assay.[42] Briefly, HeLa cells were seeded in 96-well microplates at a density of 5×10^4 cells mL^{-1} in 160 μL of cell culture medium containing 10% fetal bovine serum (FBS). After overnight culture, cells were incubated with different doses of BPH-poly(FHMA-*co*-MPC) FPNs (10-120 μg mL^{-1}) for 12 and 24 h, respectively. Then cells were washed with phosphate-buffered saline (PBS) for three times. 10 μL of CCK-8 solution and 100 μL of Dulbecco's modified eagle medium (DMEM) cell culture medium were added to each well and incubated for another 2 h at 37 ℃. Finally, plates were analyzed using a microplate reader (VictorIII, PerkinElmer). Measurements of formazan dye absorbance were carried out at 450 nm, with the reference wavelength at 620 nm. The values were proportional to the number of live cells. The percent reduction of CCK-8 dye was compared to controls (cells not exposure to BPH-poly(FHMA-*co*-MPC) FPNs), which represented 100% CCK-8 reduction. Three replicate wells were used per microplate, and the experiment was operated for three times. Cell survival was expressed as absorbance relative to that of untreated controls. Results are presented as mean ± standard deviation (SD).

2.6 Confocal microscopic imaging of BPH-poly(FHMA-*co*-MPC) FPNs

The cell uptake behavior of BPH-poly(FHMA-*co*-MPC) FPNs was investigated by a confocal laser

scanning microscope (CLSM, Zeiss 710 3-channel, Germany) using HeLa cells. The excitation wavelength was set as 405 nm. HeLa cells were set in a glass bottom dish with a density of 1×10^5 cells per dish. On the day of treatment, BPH-poly(FHMA-*co*-MPC) FPNs with a suitable concentration of 40 μg mL^{-1} was incubated with cells for 3 h at 37 °C. Afterward, the cells were washed three times with PBS to remove the redundant BPH-poly(FHMA-*co*-MPC) FPNs and then fixed with 4% paraformaldehyde for 10 min at room temperature.

3 Results and discussion

The synthetic products of each step were characterized and confirmed by ^{1}H NMR spectra. To be specific, the characteristic chemical shift of BPH located at 5.41 ppm is attributed to -NH_2 group, demonstrating the successful synthesis of BPH via Schiff base reaction (**Fig. S1**). Besides, the emerging chemical shifts of FHMA located at 6.14, 5.60 and 1.96 ppm are assigned to C=CH_2 and -CH_3 groups after CMSA reacted with methacrylic acid (**Fig. S2**). More importantly, the ^{1}H NMR spectra of monomer MPC and the purified copolymer BPH-poly(FHMA-*co*-MPC) is shown in **Fig. 1**. Obviously, the characteristic chemical shifts of the fluorescence moiety of BPH-poly(FHMA-*co*-MPC) including the protons of OH (10.18 ppm, b), CH=N (8.91 ppm, c), and aromatic ring (7.66-6.72 ppm) can be clearly observed, and the hydrophilic MPC group including the protons of N^+-CH_3 (3.31 ppm, f) and C-CH_3 (1.20 ppm, g) can also be clearly identified while the chemical shifts of 6.11 and 5.56 ppm representing the ethylene group of MPC were disappeared in BPH-poly(FHMA-*co*-MPC), demonstrating the successful RAFT polymerization and post-polymerization modification. The ^{1}H NMR results suggested the successful fabrication of the amphiphilic copolymer BPH-poly(FHMA-*co*-MPC), which was also affirmed by other techniques.

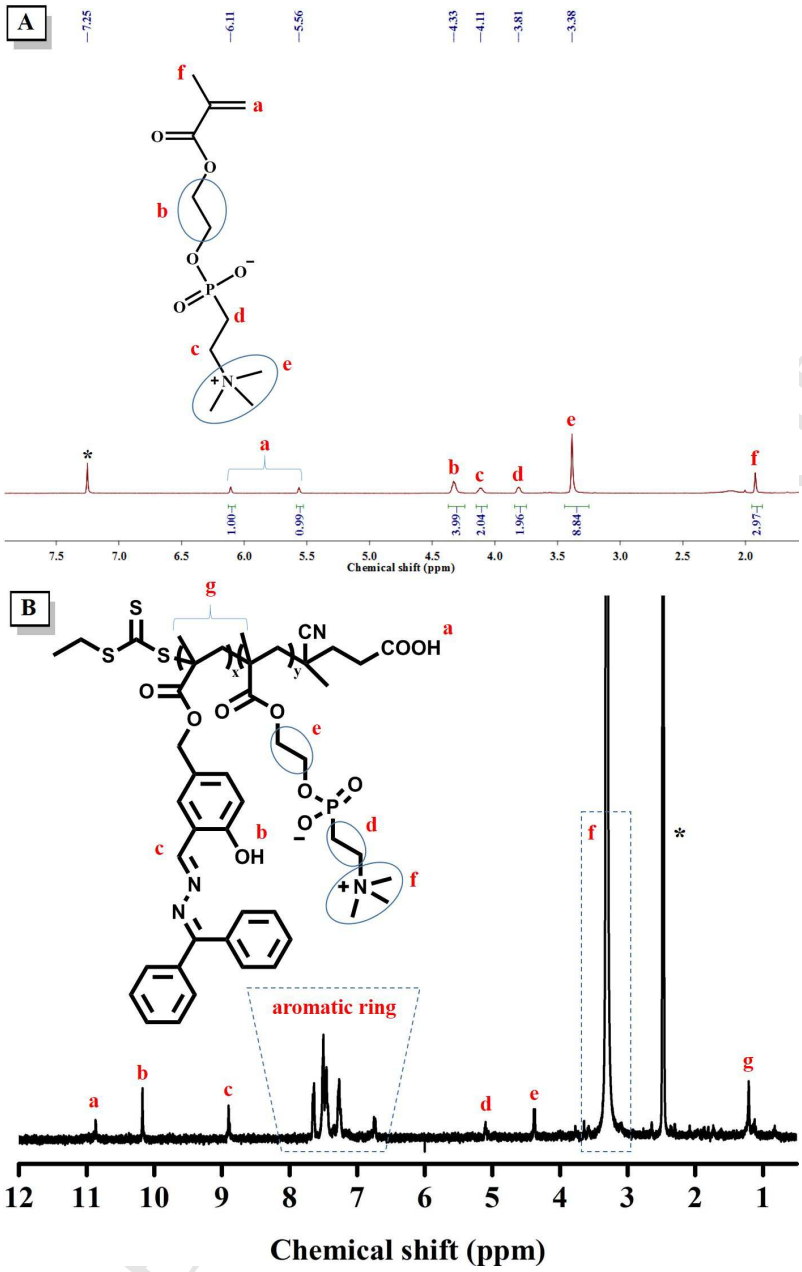

Fig. 1 ^{1}H NMR spectra of MPC and BPH-poly(FHMA-*co*-MPC). The specific NMR information about MPC, C=N and aromatic ring has been clearly indentified by ^{1}H NMR spectrum.

Furthermore, the successful synthesis of BPH, FHMA and BPH-poly(FHMA-*co*-MPC) was confirmed by FT-IR spectroscopy. Typically, two characteristic peaks of 3426 and 1629 cm^{-1} are assigned to the stretching vibration of NH_2 and C=N group, respectively, indicating the successful synthesis of BPH via Schiff base condensation (**Fig. S3**). Moreover, the strong stretching vibration bands of C=C located at 1661 cm^{-1} and C=O located at 1717 cm^{-1} were found in FHMA when CMSA reacted with methacrylic acid, which suggested its successful synthesis (**Fig. 2A**). More importantly, compared with the FT-IR spectrum of FHMA, a new characteristic peak of 1590 cm^{-1} attributed to the

stretching vibration of C=N is highlighted and the stretching vibration of C=C is disappeared in as-prepared BPH-poly(FHMA-*co*-MPC), indicating the successful polymerization of CMSA and MPC and further post-polymerization modification via Schiff base condensation (**Fig. 2B**). Combined the results of ^{1}H NMR spectra and FT-IR spectra, we can draw a conclusion that the zwitterionic copolymer BPH-poly(FHMA-*co*-MPC) was synthesized successfully.

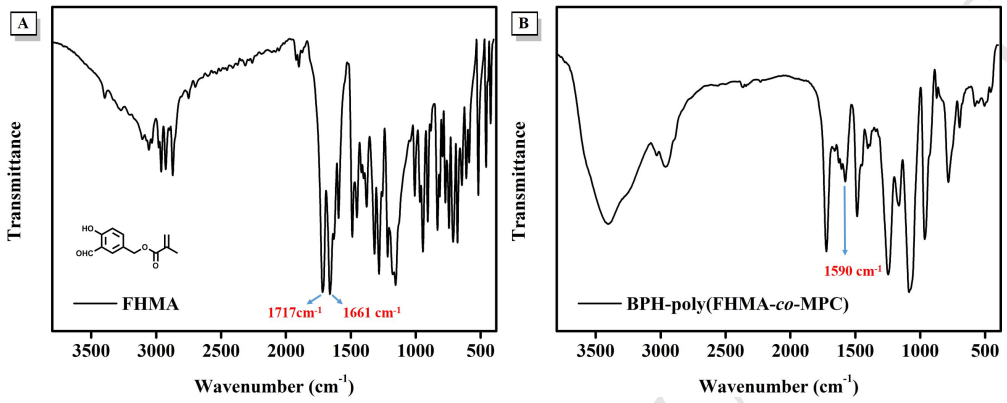

Fig. 2 FT-IR spectra of FHMA and BPH-poly(FHMA-*co*-MPC).

According to the previous reports, amphiphilic copolymers tend to form nanoparticles with a hydrophobic core and a hydrophilic shell in aqueous environments through self-assembly strategy.[43] Therefore, the morphology and size of BPH-poly(FHMA-*co*-MPC) FPNs were characterized by TEM and DLS. As shown in **Fig. 3A**, lots of spherical nanoaggregates with diameters ranging about 100 nm are observed, indicating the formation of nanoparticles via self-assembly when the as-prepared amphiphilic copolymer BPH-poly(FHMA-*co*-MPC) dispersed in water. Furthermore, the hydrodynamic size distribution of BPH-poly(FHMA-*co*-MPC) FPNs suggested that the size of these FPNs in water is in the range of 50–200 nm (**Fig. 3B**). It is noteworthy that the size of BPH-poly(FHMA-*co*-MPC) FPNs characterized by TEM is somewhat smaller than the hydrodynamic size, which might be due to the shrinkage of micelle for TEM observation. Hence, the above results demonstrated that BPH-poly(FHMA-*co*-MPC) FPNs possess suitable size and excellent water dispersibility, implying their potential for biomedical applications.

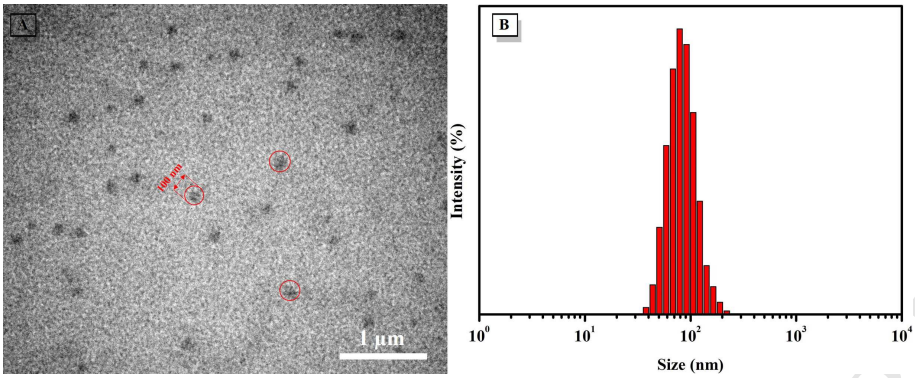

Fig. 3 (A) TEM image of BPH-poly(FHMA-*co*-MPC) FPNs dispersed in water, revealing spherical nanoparticle morphology; (B) Size distribution of BPH-poly(FHMA-*co*-MPC) FPNs dispersed in water determined by DLS.

The chemical composition of BPH-poly(FHMA-*co*-MPC) was analyzed by XPS spectrum. Carbon (C), oxygen (O), nitrogen (N), phosphorus (P) and sulfur (S) elements are presented in low-resolution XPS spectrum of BPH-poly(FHMA-*co*-MPC) (**Fig. 4**). **Table S1** shows that the overall wt % of these elements (C: O: N: P: S) as 71.74: 19.39: 5.89: 2.49: 0.49, respectively. The element S should be derived from the CTA, while the element P should be originated from the MPC. The element N should be derived both from the MPC and Schiff base. Moreover, based on the element ratio values, we could clearly find that the content of N is obviously greater than that of P. This implied that the final copolymers contain both MPC and Schiff base. And the molar ratio of Schiff base to MPC is 0.683:1. All of the above results indicated that we have successfully synthesized the AIE-active polymers through the combination of RAFT polymerization and post-polymerization modification (formation of Schiff base).

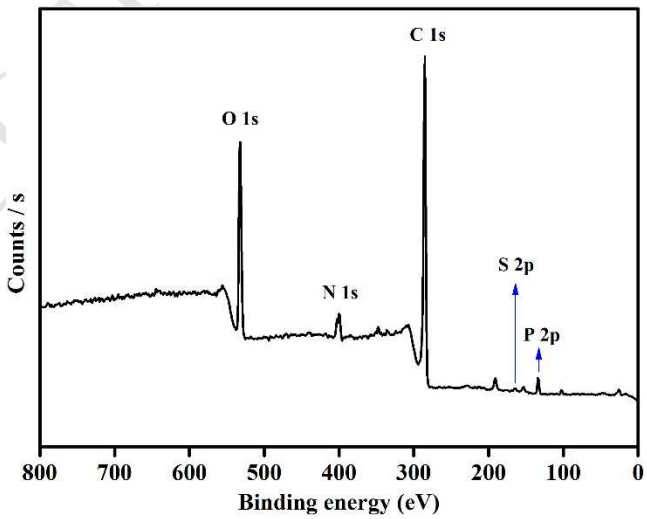

Fig. 4 XPS spectrum of BPH-poly(FHMA-*co*-MPC) with different components of carbon (C), oxygen (O), nitrogen (N), phosphorus (P) and sulfur (S) elements.

High-resolution spectra of C 1s of BPH-poly(FHMA-*co*-MPC) is split into four main components: -CH group at ~285 eV, C-O or C-N groups at 286 eV, and C=O group at 287 eV, respectively (**Fig. 5A**). Several peaks that centered at 532.4 and 530.6 eV are found in the high-resolution spectrum of O 1s. These peaks indicated that the atom O is conjugated with different elements (P, C). More importantly, binding energies of C-N^+ and C=N bond of the region N 1s in BPH-poly(FHMA-*co*-MPC) are 402.7 eV and 399.3 eV, respectively, which suggested BPH was conjugated with salicylaldehyde (SA)-functional preliminary copolymer via Schiff base condensation (**Fig. S5**).[44] Final, the existence of P and S also suggested that the copolymers were obtained through RAFT polymerization.

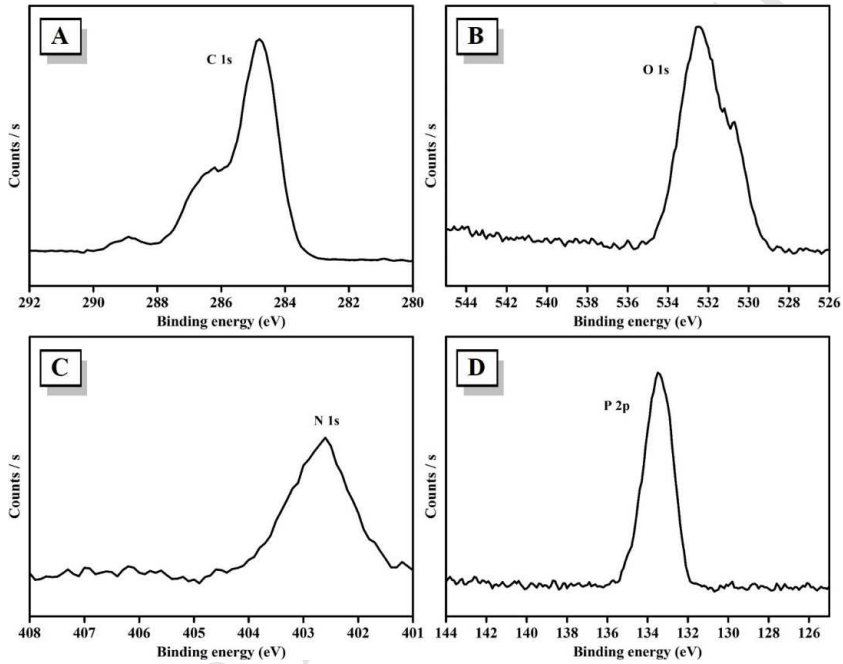

Fig. 5 High-resolution spectra of BPH-poly(FHMA-*co*-MPC). (A) The region of C1s, (B) The region of O 1s, (C) The region of N 1s, (D) The region of P 2p.

Due to the amphiphilic properties, BPH-poly(FHMA-*co*-MPC) copolymers self-assemble in aqueous solution with the hydrophobic fluorescent moieties aggregating together to form the core and the hydrophilic MPC chains extended towards the aqueous solution. Thus obtained BPH-poly(FHMA-*co*-MPC) FPNs are endowed with good water dispersibility. It can be seen that no obvious precipitation and the background character “Nanchang University” could be observed when BPH-poly(FHMA-*co*-MPC) FPNs were dispersed in water (inset of **Fig. 6A**). The UV absorption spectrum of BPH-poly(FHMA-*co*-MPC) FPNs in water is shown in **Fig. 6A**, two peaks located at 306 and 352 nm could be found. The strong absorption peak at 306 nm could be attributed to $\pi \rightarrow \pi^*$ transition, which demonstrated the existence of conjugated chemical structure of

BPH-poly(FHMA-*co*-MPC) FPNs. Furthermore, it can be concluded that aromatic rings have been conjugated with hetero atom such as N of BPH-poly(FHMA-*co*-MPC) FPNs because a shoulder peak at 352 nm could be ascribed to the R band of n→π* transition. Intense yellow fluorescence can be observed from the BPH-poly(FHMA-*co*-MPC) FPNs after they were irradiated by a UV-lamp at 365 nm (inset of **Fig. 6B**). Fluorescence (FL) spectra shown in **Fig. 6B** indicated that the maximum emission wavelength is located at 546 nm when BPH-poly(FHMA-*co*-MPC) FPNs in water were excited with 405 nm wavelength. More importantly, the fluorescence stability of ~~was~~ BPH-poly(FHMA-*co*-MPC) FPNs was also examined. As displayed in **Fig. 6C**, even though BPH-poly(FHMA-*co*-MPC) FPNs suspension were irradiated at 365 nm for 1 h, no obvious decrease in FL intensity was observed. It can be seen that the fluorescence intensity after irradiation is still greater than 95% as compared with the value before irradiation. It suggests that BPH-poly(FHMA-*co*-MPC) FPNs possess desirable photo-bleaching resistance. The AIE properties of BPH-poly(FHMA-*co*-MPC) FPNs could be determined by good and poor solvents because the obtain BPH-poly(FHMA-*co*-MPC) copolymers could dissolve well in some organic solvents such as DMF while just dispersed in aqueous solution. As shown in **Fig. 6D**, no fluorescence could be observed when BPH-poly(FHMA-*co*-MPC) copolymers were dissolved in DMF while bright yellow fluorescent could be observed with a maximum emission peak at 546 nm, indicating obvious AIE properties. The mechanism of the AIE properties for BPH-poly(FHMA-co-MPC) copolymers could be explained in a similar manner to previous literatures.[45-47] In solution state, nonradiative relaxation of the excited states was activated by the free intermolecular rotation around the N-N bond, resulting in fluorescence quenching. However, after BPH-poly(FHMA-co-MPC) copolymers self-assemble in aqueous solution, the rotation was inhibited in the aggregate state, which demonstrate their AIE attributes and the excited state intramolecular proton transfer (ESIPT) fluorescence.

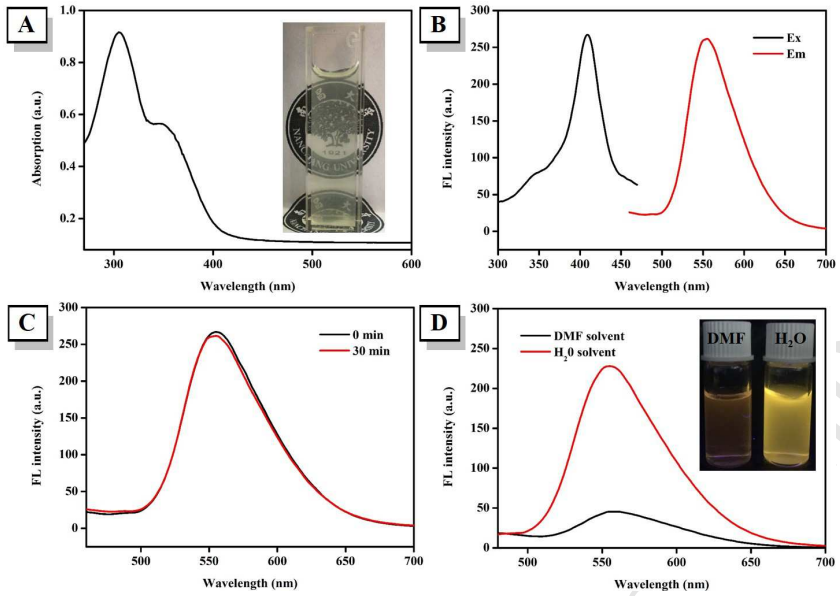

Fig. 6 (A) The UV absorption spectrum of BPH-poly(FHMA-*co*-MPC) FPNs in water. Inset: visible photograph of BPH-poly(FHMA-*co*-MPC) FPNs in water using the logo of "Nanchang University" as background; (B) The FL spectra of BPH-poly(FHMA-*co*-MPC) FPNs in water. Inset: FL image of BPH-poly(FHMA-*co*-MPC) FPNs in water taken at 365 nm UV light; (C) FL stability of BPH-poly(PEG-*co*-FHMA) FPNs under continuous UV light exposure of 365 nm for 1 h; (D) The FL emission spectra of BPH-poly(FHMA-*co*-MPC) FPNs in DMF and water. Inset: FL images of BPH-poly(FHMA-*co*-MPC) FPNs in DMF (left) and water (right) taken at 365 nm UV light.

The critical micelle concentration (CMC) is the minimum concentration of surfactant or amphiphilic polymers required for micelles to form, which is highly important for the construction of stable micelles in low concentration of solution. Thus, the CMC value of the BPH-poly(FHMA-*co*-MPC) FPNs was determined by conducting the FL spectra of BPH-poly(FHMA-*co*-MPC) FPNs in water at different concentrations, with excitation wavelength was 405 nm (**Fig. 7A**). Furthermore, the intensity of the fluorescence emission vs. the logarithm of the concentration of BPH-poly(FHMA-*co*-MPC) FPNs was plotted to determine the CMC by the tangent method (**Fig. 7B**). The results suggested that the CMC value of BPH-poly(FHMA-*co*-MPC) FNPs is 0.033 mg mL^{-1}. Therefore, the BPH-poly(FHMA-*co*-MPC) FNPs with low CMC value would be stable under diluent physiological conditions and useful for practical applications.

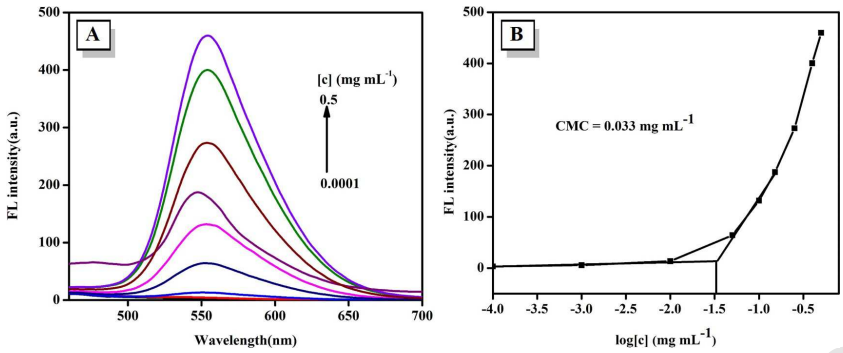

Fig. 7 (A) FL spectra of BPH-poly(FHMA-*co*-MPC) FPNs in water at different concentrations (0.0001-0.5 mg mL^{-1}), excitation wavelength was 402 nm. (B) The relationship of the FL intensity and the logarithm of BPH-poly(FHMA-*co*-MPC) FPNs concentration in water.

All above characterization results suggested BPH-poly(FHMA-*co*-MPC) FPNs possess good water dispersibility, desirable particle size and unique photophysical properties, which seem to suitable for bioimaging applications. However, biocompatibility evaluation is a necessary step before evaluating the potential biomedical applications of BPH-poly(FHMA-*co*-MPC) FPNs. As shown in **Fig. 8**, it is worth mentioning that only little decrease of cell viability value after the cells were incubated with BPH-poly(FHMA-*co*-MPC) FPNs at different concentrations for 12 h and 24 h. Moreover, the cell viability value is still greater than 95% after 24 h incubation even the concentrations of BPH-poly(FHMA-*co*-MPC) FPNs as high as 120 μg mL^{-1}, suggesting that excellent biocompatibility of BPH-poly(FHMA-*co*-MPC) FPNs. It could draw a preliminary conclusion that BPH-poly(FHMA-*co*-MPC) FPNs have great potential in cell imaging application.

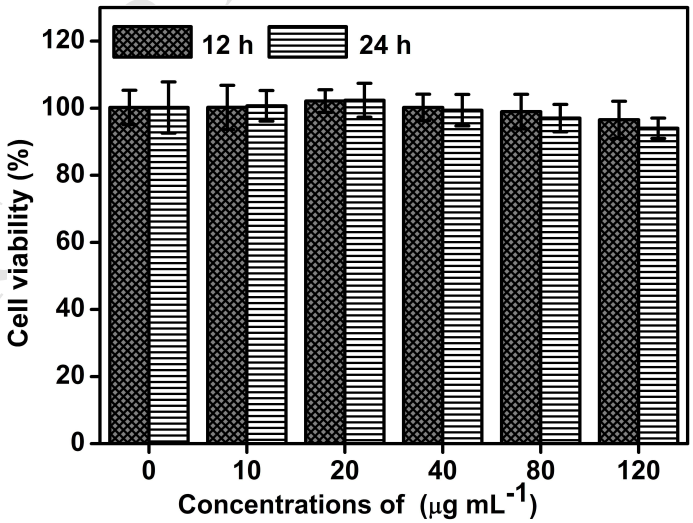

Fig. 8 Cell viability of BPH-poly(FHMA-*co*-MPC) FPNs with HeLa cells for 12 h and 24 h, respectively.

On the basis of excellent biocompatibility, the cellular uptake of BPH-poly(FHMA-*co*-MPC) FPNs was investigated by CLSM. Bright field of CLSM image shown in **Fig. 9A** revealed that cells still keep their normal morphology after they were incubated with 40 μg mL^{-1} of BPH-poly(FHMA-*co*-MPC) FPNs for 3 h, further demonstrating their good biocompatibility. Moreover, many dark areas are surrounded by intense yellow fluorescence, which suggested that BPH-poly(FHMA-*co*-MPC) FPNs are internalized by HeLa cells ~~via phagocytosis~~ and mainly distributed in the whole cytoplasm (**Fig. 9B**). These dark areas should be the locations of cell nuclei because the size of BPH-poly(FHMA-*co*-MPC) FPNs is obvious larger than that of nucleus pores and therefore could not enter into cell nuclei. **Fig. 9C** shows the merged image of bright field and fluorescent images. It can be seen that the fluorescence signals are almost overlaid with the cell locations. It further indicated that the BPH-poly(FHMA-*co*-MPC) FPNs are internalized ~~through non-specific route~~. Combine the above cell viability results so we can draw a concluded that BPH-poly(FHMA-*co*-MPC) FPNs have great potential for practical biological imaging.

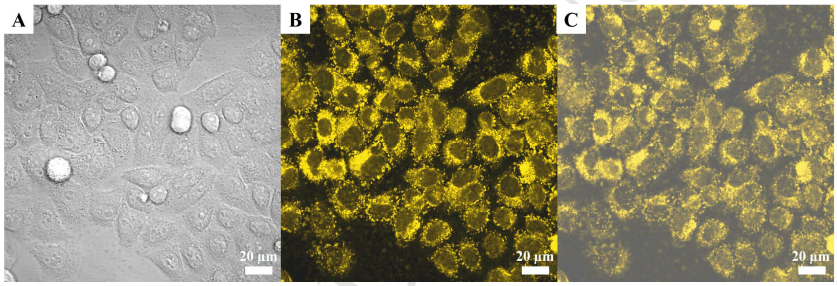

Fig. 9 CLSM images of HeLa cells incubated with 40 μg mL^{-1} of BPH-poly(FHMA-*co*-MPC) FPNs for 3 h. (A) Bright field, (B) excited with 405 nm laser, (C) merge image of A and B. Scale bar = 20 μm.

4 Conclusions

In summary, we have developed a novel strategy for preparation of BPH-poly(FHMA-*co*-MPC) FPNs through the combination of RAFT polymerization and post-polymerization modification. The resultant BPH-poly(FHMA-*co*-MPC) FPNs showed numerous excellent properties such as high water dispersibility, uniform morphology, intense yellow fluorescence, large Stokes shifts, remarkable photostability and excellent biocompatibility, making them promising for biological imaging applications. Compared with the construction of AIE-active FPNs based on polymerizable or functionalized AIE molecules, the novel method provided by this contribution has many advantages. First, it can avoid the complex process for the synthesis of AIE dyes. Secondly, the chemical composition and fluorescence properties and the physicochemical properties of copolymers can be facilely adjusted via the RAFT polymerization and Schiff base reaction. More importantly, this work

provides novel ideas for the fabrication of AIE-active FPNs through the post-polymerization modification.

Acknowledgements

This research was supported by the National Natural Science Foundation of China (Nos. 51363016, 21474057, 21564006, 21561022, 21644014), Natural Science Foundation of Jiangxi Province in China (Nos. 20161BAB203072, 20161BAB213066).

References

[1] Mei J, Leung NL, Kwok RT, Lam JW, Tang BZ. Aggregation-induced emission: together we shine, united we soar! Chem Rev. 2015;115(21):11718-940.

[2] Yao J, Yang M, Duan Y. Chemistry, biology, and medicine of fluorescent nanomaterials and related systems: new insights into biosensing, bioimaging, genomics, diagnostics, and therapy. Chem Rev. 2014;114(12):6130-78.

[3] Li K, Liu B. Polymer-encapsulated organic nanoparticles for fluorescence and photoacoustic imaging. Chem Soc Rev. 2014;43(18):6570-97.

[4] Liu M, Zeng G, Wang K, Wan Q, Tao L, Zhang X, et al. Recent developments in polydopamine: an emerging soft matter for surface modification and biomedical applications. Nanoscale. 2016;8(38):16819-40.

[5] Hong Y, Lam JW, Tang BZ. Aggregation-induced emission. Chem Soc Rev. 2011;40(11):5361-88.

[6] Luo J, Xie Z, Lam JW, Cheng L, Chen H, Qiu C, et al. Aggregation-induced emission of 1-methyl-1, 2, 3, 4, 5-pentaphenylsilole. Chem Commun. 2001(18):1740-1.

[7] Mei J, Hong Y, Lam JW, Qin A, Tang Y, Tang BZ. Aggregation‐induced emission: the whole is more brilliant than the parts. Adv Mater. 2014;26(31):5429-79.

[8] Nie H, Hu K, Cai Y, Peng Q, Zhao Z, Hu R, et al. Tetraphenylfuran: aggregation-induced emission or aggregation-caused quenching? Mater Chem Front. 2017;1(6):1125-9.

[9] Ding D, Li K, Liu B, Tang BZ. Bioprobes based on AIE fluorogens. Accounts Chem Res. 2013;46(11):2441-53.

[10] Zhan C, You X, Zhang G, Zhang D. Bio‐/Chemosensors and Imaging with Aggregation‐Induced Emission Luminogens. Chem Rec. 2016;16(4):2142-60.

[11] Hu R, Leung NL, Tang BZ. AIE macromolecules: syntheses, structures and functionalities. Chem Soc Rev. 2014;43(13):4494-562.

[12] Leung CWT, Hong Y, Chen S, Zhao E, Lam JWY, Tang BZ. A photostable AIE luminogen for specific mitochondrial imaging and tracking. J Am Chem Soc. 2012;135(1):62-5.

[13] Wang Z, Chen S, Lam JW, Qin W, Kwok RT, Xie N, et al. Long-term fluorescent cellular tracing by the aggregates of AIE bioconjugates. J Am Chem Soc. 2013;135(22):8238-45.

[14] Shi H, Kwok RT, Liu J, Xing B, Tang BZ, Liu B. Real-time monitoring of cell apoptosis and drug screening using fluorescent light-up probe with aggregation-induced emission characteristics. J Am Chem Soc. 2012;134(43):17972-81.

[15] Shi H, Liu J, Geng J, Tang BZ, Liu B. Specific detection of integrin αvβ3 by light-up bioprobe with aggregation-induced emission characteristics. J Am Chem Soc. 2012;134(23):9569-72.

[16] Feng L, Wang C, Deng X, Miao X, Wang J, Wang Y, et al. New application of AIEgens realized in photodetectors: reduced work function of transparent electrodes and much improved performance. Mater Chem Front. 2018.

[17] Zhang X, Wang K, Liu M, Zhang X, Tao L, Chen Y, et al. Polymeric AIE-based nanoprobes for biomedical applications: recent advances and perspectives. Nanoscale. 2015;7(27):11486-508.

[18] Zhan R, Pan Y, Manghnani PN, Liu B. AIE Polymers: Synthesis, Properties, and Biological Applications. Macromol Biosci. 2017;17(5).

[19] Cao Z, Liang X, Chen H, Gao M, Zhao Z, Chen X, et al. Bright and biocompatible AIE polymeric nanoparticles prepared from miniemulsion for fluorescence cell imaging. Polym Chem. 2016;7(35):5571-8.

[20] Li C, Liu X, He S, Huang Y, Cui D. Synthesis and AIE properties of PEG–PLA–PMPC based triblock amphiphilic biodegradable polymers. Polym Chem. 2016;7(5):1121-8.

[21] Zhang X, Zhang X, Wang S, Liu M, Tao L, Wei Y. Surfactant modification of aggregation-induced emission material as biocompatible nanoparticles: Facile preparation and cell imaging. Nanoscale. 2013;5(1):147-50.

[22] Zhang X, Zhang X, Yang B, Zhang Y, Liu M, Liu W, et al. Fabrication of water-dispersible and biocompatible red fluorescent organic nanoparticles via PEGylation of aggregate induced emission enhancement dye and their cell imaging applications. Colloid Surfaces B. 2014;113:435-41.

[23] Shen X, Shi Y, Peng B, Li K, Xiang J, Zhang G, et al. Fluorescent Polymeric Micelles with Tetraphenylethylene Moieties and Their Application for the Selective Detection of Glucose. Macromol Biosci. 2012;12(11):1583-90.

[24] Yuan Y, Xu S, Zhang C-J, Liu B. Light-responsive AIE nanoparticles with cytosolic drug release to overcome drug resistance in cancer cells. Polym Chem. 2016;7(21):3530-9.

[25] Zhang J, Zhu J, Lu C, Gu Z, He T, Yang A, et al. A hyperbranched fluorescent supramolecular polymer with aggregation induced emission (AIE) properties. Polym Chem. 2016;7(26):4317-21.

[26] Tian J, Jiang R, Gao P, Xu D, Mao L, Zeng G, et al. Synthesis and cell imaging applications of amphiphilic AIE-active poly (amino acid) s. Mater Sci Eng C-Mater. 2017;79:563-9.

[27] Ma C, Xie G, Zhang X, Yang L, Li Y, Liu H, et al. Biocompatible fluorescent polymers from PEGylation of an aggregation-induced emission dye. Dyes Pigments. 2017;139:672-80.

[28] Ma C, Zhang X, Yang L, Li Y, Liu H, Yang Y, et al. Alkyl length dependent mechanofluorochromism of AIE-based phenothiazinyl fluorophenyl acrylonitrile derivatives. Dyes Pigments. 2017;136:85-91.

[29] Xie G, Ma C, Zhang X, Liu H, Yang L, Li Y, et al. Chitosan-based cross-linked fluorescent polymer containing aggregation-induced emission fluorogen for cell imaging. Dyes Pigments. 2017;143:276-83.

[30] Wan Q, Jiang R, Mao L, Xu D, Zeng G, Shi Y, et al. A powerful “one-pot” tool for fabrication of AIE-active luminescent organic nanoparticles through the combination of RAFT polymerization and multicomponent reactions. Mater Chem Front. 2017;1(6):1051-8.

[31] Gauthier MA, Gibson MI, Klok HA. Synthesis of Functional Polymers by Post‐Polymerization Modification. Angew Chem. 2009;48(1):48-58.

[32] Ghosh S, Basu S, Thayumanavan S. Simultaneous and reversible functionalization of copolymers for biological applications. Macromolecules. 2006;39(17):5595-7.

[33] Zhang J, Wang L, Li C, Li Y, Liu J, Tu Y, et al. Preparation and characterization of solution processable phthalocyanine‐containing polymers via a combination of RAFT polymerization and post‐polymerization modification techniques. J Polym Sci Pol Chem. 2014;52(5):691-8.

[34] Fokina A, Lee Y, Chang JH, Braun L, Bae WK, Char K, et al. Side-chain conjugated polymers for use in the active layers of hybrid semiconducting polymer/quantum dot light emitting diodes. Polym Chem. 2016;7(1):101-12.

[35] Boaen NK, Hillmyer MA. Post-polymerization functionalization of polyolefins. Chem Soc Rev.

2005;34(3):267-75.

[36] Gupta K, Sutar AK. Catalytic activities of Schiff base transition metal complexes. Coordin Chem Rev. 2008;252(12-14):1420-50.

[37] Katsuki T. Unique asymmetric catalysis of cis-β metal complexes of salen and its related Schiff-base ligands. Chem Soc Rev. 2004;33(7):437-44.

[38] Cozzi PG. Metal–Salen Schiff base complexes in catalysis: practical aspects. Chem Soc Rev. 2004;33(7):410-21.

[39] Adsule S, Barve V, Chen D, Ahmed F, Dou QP, Padhye S, et al. Novel Schiff base copper complexes of quinoline-2 carboxaldehyde as proteasome inhibitors in human prostate cancer cells. J Med Chem. 2006;49(24):7242-6.

[40] Tao L, Liu J, Davis TP. Branched Polymer− Protein Conjugates Made From Mid-Chain-Functional P (HPMA). Biomacromolecules. 2009;10(10):2847-51.

[41] Bagherzadeh M, Zare M. Synthesis, characterization, and catalysis of recyclable new piperazine-bridged Mo (VI) polymers [MoO2 (Salen)(piperazine)] n in highly selective oxygenation of alkenes and sulfides. J Coord Chem. 2013;66(16):2885-900.

[42] Zhang X, Hu W, Li J, Tao L, Wei Y. A comparative study of cellular uptake and cytotoxicity of multi-walled carbon nanotubes, graphene oxide, and nanodiamond. Toxicol Res. 2012;1(1):62-8.

[43] Zhang X, Zhang X, Tao L, Chi Z, Xu J, Wei Y. Aggregation induced emission-based fluorescent nanoparticles: fabrication methodologies and biomedical applications. J Mater Chem B. 2014;2(28):4398-414.

[44] He W, Jiang C, Wang J, Lu L. High‐Rate Oxygen Electroreduction over Graphitic‐N Species Exposed on 3D Hierarchically Porous Nitrogen‐Doped Carbons. Angew Chem Int Edit. 2014;53(36):9503-7.

[45] Peng L, Wei R, Li K, Zhou Z, Song P, Tong A. A ratiometric fluorescent probe for hydrophobic proteins in aqueous solution based on aggregation-induced emission. Analyst. 2013;138(7):2068-72.

[46] Wei R, Song P, Tong A. Reversible thermochromism of aggregation-induced emission-active benzophenone azine based on polymorph-dependent excited-state intramolecular proton transfer fluorescence. J Phys Chem C. 2013;117(7):3467-74.

[47] Wang Z, Gui C, Zhao E, Wang J, Li X, Qin A, et al. Specific fluorescence probes for lipid droplets based on simple AIEgens. ACS Appl Mater Inter. 2016;8(16):10193-200.

- ► Fluorescent polymeric nanoparticles with aggregation-induced emission feature
- ► AIE-active FPNs through formation of Schiff base
- ► The method for preparation of AIE-active FPNs is rather simple and effective
- ► These AIE-active FPNs are promising for biomedical applications